Combustion Theory and Modelling, 2020
https://doi.org/10.1080/13647830.2020.1780325

Effects of pressure rise rate on laminar flame speed under normal and engine-relevant conditions

Yiqing Wang[a], Jagannath Jayachandran[b] and Zheng Chen [a]*

[a]*SKLTCS, CAPT, BIC-ESAT, Department of Mechanics and Engineering Science, College of Engineering, Peking University, Beijing, People's Republic of China;* [b]*Aerospace Program, Department of Mechanical Engineering, Worcester Polytechnic Institute, Worcester, MA, USA*

(*Received 17 November 2019; accepted 27 May 2020*)

Laminar flame speed (LFS) is one of the most important physicochemical properties of a combustible mixture. At normal and elevated temperatures and pressures, LFS can be measured using propagating spherical flames in a closed chamber. LFS is also used in certain turbulent premixed flame modelling for combustion in spark ignition engines. Inside the closed chamber or engine, transient pressure rise occurs during the premixed flame propagation. The effects of pressure rise rate (PRR) on LFS are examined numerically in this study. One-dimensional simulations are conducted for spherical flame propagation in a closed chamber. Detailed chemistry and transport are considered. Different values of PRR at the same temperature and pressure are achieved through changing the spherical chamber size. It is found that the effect of PRR on LFS is negligible under the normal and engine-relevant conditions considered in this study. This observation is then explained through the comparison between the unsteady and convection terms in the energy equation for a premixed flame.

Keywords: laminar flame speed; pressure rise rate; constant-volume propagating spherical flame; engine-relevant conditions

1. Introduction

Laminar flame speed (LFS) is a fundamental physicochemical property of a combustible mixture. Ideally, it is defined for a planar, unstretched, adiabatic, premixed flame [1]. However, in reality the premixed flame is affected by different factors such as curvature, strain, heat loss, etc. Therefore, the LFS should be measured after correcting the influence due to these factors [2–4]. For example, in counterflow flame and propagating spherical flame experiments, the LFS should be obtained from extrapolation to zero stretch rate [2–9]. The effects of curvature, strain and heat loss on LFS have been extensively studied ([2–4,7,10–12] and references therein). However, according to Clavin and Joulin [13] the unsteady pressure change might also affect the premixed flame speed. They proposed the following expression for the deviation of local flame speed, S_u, from the ideal LFS, S_u^0,

$$S_u = S_u^0 - (L_S K_S + L_C K_C + L_P K_P + \ldots), \tag{1}$$

where K_S and K_C respectively represent the stretch rate due to strain rate and curvature [6,14], and $K_P = (1/P)(\mathrm{d}P/\mathrm{d}t)$ is the relative Pressure Rise Rate (PRR). L_s, L_c and L_P are the corresponding Markstein lengths [13].

*Corresponding author. Email: cz@pku.edu.cn

Usually, only the effects of strain and curvature in Equation (1) are considered; while the effect of PRR is neglected. However, for premixed flame propagation inside a closed vessel, the PRR can be very large and it might affect the LFS [13]. Currently, the constant-volume propagating spherical flame method is popularly used to measure the LFS (e.g., [15–23]). In this method, the flame is center-ignited inside a closed spherical chamber and then the temporal evolution of pressure rise during the spherical flame propagation is recorded. The LFS is obtained from the pressure history. There are many studies (see [24] and references therein) on different factors which affect the accuracy of LFS measured from this method. However, the effects of PRR have not been systematically examined. This brings the first question: does the unsteady pressure rise affect the LFS measured from the constant-volume propagating spherical flame method?

Furthermore, there is high PRR (10^4–10^5 atm/s) and high relative PRR (10^3–10^4 s^{-1}) during the premixed turbulent flame propagation in spark ignition engines (SIEs). The LFS is used as an input in certain turbulent premixed combustion modelling for SIEs (e.g., the level-set combustion model used in [25,26]). However, in such type of turbulent combustion modelling, the effect of PRR on the LFS has not been considered before. The effect of PRR on flame propagation needs to be investigated at engine-relevant thermodynamic conditions as well as PRRs. Recently, Jayachandran and Egolfopoulos [27] have developed a numerical model to parametrically study the effect of PRR on flame propagation for the first time. The effect of PRR on flame speed was quantified through the Pressure Rise Number (PRN_f), which is the ratio between the flame propagation time scale and the pressure rise time scale. They found a significant increase in mass burning flux with PRN_f, i.e. mass burning rate increases relative to the steady state (PRR = 0) value for increasing values of PRR. However, the range of PRR considered in their work is very large while the initial temperature and pressure are still below engine-relevant conditions. Therefore, the second question is whether the PRR affects the premixed flame propagation under engine-relevant conditions.

This work aims to answer these two questions by assessing the effects of PRR on LFS under normal and engine-relevant conditions. First, 1D simulations are conducted for spherical flame propagation in a closed chamber, and the LFSs at different values of PRR are obtained and compared. Then, the unsteady effects are analyzed based on the energy equation for a premixed flame, which helps to explain the simulation results.

It is noted that the pressure itself affects the LFS, and that the expansion or compression with pressure variation can change the LFS mainly due to the change in the temperature of unburned gas. For example, laminar flame propagation in a confined vessel can be quenched by rapid pressure decrease as observed in experiments [28] and theoretical analysis [29]. Unlike those studies, in this work the LFSs at the same temperature and pressure of the same unburned mixture but different PRRs are studied.

2. Numerical model and methods

Here we consider 1D spherical flame propagation in a closed chamber. The constant-volume propagating spherical flame method [12] introduced before is used to get LFS. From the pressure history, $P = P(t)$, we can determine the local LFS, S_u, according to:

$$S_u = \frac{R_W}{3}\left[1-(1-x)\left(\frac{P_0}{P}\right)^{1/\gamma_u}\right]^{-2/3}\left(\frac{P_0}{P}\right)^{1/\gamma_u}\frac{\mathrm{d}x}{\mathrm{d}t}, \tag{2}$$

where R_W is the inner radius of the closed chamber, x the burnt mass fraction, P_0 the initial pressure, and γ_u the heat capacity ratio of unburned gas. Details on this method and derivation of Equation (2) can be found in the Supplementary Document or Ref. [12].

The constant-volume propagating spherical flame method has the advantage in obtaining the LFS at a broad range of temperature and pressure [14]. In simulation, radiation is not considered and thereby its effects on LFS [15–17] are excluded. Besides, as shown in the Supplementary Document, the influence of stretch on LFS is within 0.5% and thereby negligible. Therefore, the effects of PRR on LFS are isolated and can be quantified. It is noted that a small chamber radius of $R_W = 1$ cm is used here to achieve large PRR; while in practical constant-volume propagating spherical flame experiments, the chamber radius is usually above 5 cm [12]. Since the heat loss to wall is not considered in simulation, the influence of thermal boundary layer in the inner chamber is circumvented.

The in-house code A-SURF (Adaptive Simulation of Unsteady Reactive Flow) [30–32] is used to simulate the 1D spherical flame propagation in a closed chamber. The conservation equations for compressible, multi-component, reactive flow are solved using the finite volume method. Three fuels, hydrogen, methane and isooctane, are considered and the detailed chemical mechanisms [33–35] are used. The computational domain is initially filled with static fuel/air mixture at the initial temperature and pressure denoted as $T_{u,0}$ and P_0, respectively. Zero flow speed and zero gradients for temperature and mass fractions are enforced at both boundaries. The flame is centrally initiated by a hot spot. To accurately resolve the propagating flame front, adaptive mesh refinement is used. At high pressure up to 90 atm, the reaction zone is always covered by the finest mesh with the width of 0.12 μm. Grid convergence is ensured. A-SURF has been used to simulate ignition and flame propagation in previous studies (e.g., [36–40]). The details on governing equations and numerical methods are presented in [30–32].

3. Dependence of relative PRR on chamber size

To quantify the effects of PRR on LFS, we need compare the LFSs at different values of PRR while maintaining the same temperature and pressure for the unburned mixture. According the analysis in the Supplementary Document, we have following relationship between the relative PRR, K_P, and chamber radius, R_W:

$$K_P = \frac{3S_u}{R_W}\frac{(P_e - P)}{P}\left(\frac{P}{P_0}\right)^{1/\gamma_u}\left(\frac{R_f}{R_W}\right)^2, \tag{3}$$

where P_0 and P_e are respectively the initial and final chamber pressures. P and S_u are respectively the pressure and local LFS at the time when the flame radius is R_f. The normalized flame radius, R_f/R_W, only depends on the pressure P [29]:

$$\frac{R_f}{R_W} = \left[1 - \left(\frac{P_e - P}{P_e - P_0}\right)\left(\frac{P_0}{P}\right)^{1/\gamma_u}\right]^{1/3}, \tag{4}$$

The flame speed, S_u, mainly depends on the temperature, T_u, and pressure, P, of the unburnt gas, i.e., $S_u = S_u(T_u, P)$. Due to the isentropic-compression relationship,

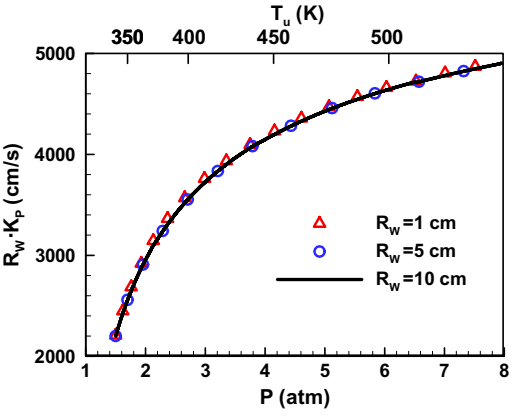

Figure 1. Change of the product of chamber radius and relative PRR, $R_W \cdot K_P$, with pressure, P, and temperature, T_u, of unburned gas during spherical flame propagation in stoichiometric H_2/air initially at $T_{u,0} = 300\,\text{K}$ and $P_0 = 1\,\text{atm}$.

$T_u/T_{u,0} = (P/P_0)^{(1-1/\gamma_u)}$, we have $S_u = S_u(P)$. Therefore, Equation (3) reduces to:

$$K_P = f(P)/R_W \tag{5}$$

where $f(P)$ is a function of pressure, P, and it monotonically increases during spherical flame propagating inside the closed chamber.

According to Equation (5), the relative PRR at some specific pressure is inversely proportional to the chamber size. This is demonstrated by Figure 1, which shows the product, $R_W.K_P$, is nearly the same for three chamber sizes of $R_W = 1$, 5 and 10 cm. At one specific pressure, the unburned gas temperature is determined by the relationship, $T_{u/}/T_{u,0} = (P/P_0)^{(1-1/\gamma_u)}$. Therefore, different values of relative PRR at the same temperature and pressure can be achieved through changing the spherical chamber size. Figure 1 also shows that the highest relative PRR is only around $1000\,\text{s}^{-1}$ for $R_W = 5\,\text{cm}$ while it is close to $5000\,\text{s}^{-1}$ for $R_W = 1\,\text{cm}$. Therefore, a high relative PRR can be achieved by reducing the chamber size. It is noted that a small chamber radius of $R_W = 1\,\text{cm}$ is used here to achieve large PRR; while in practical constant-volume propagating spherical flame experiments, the chamber radius is usually above 5 cm [24].

4. Numerical results on LFSs at different PRRs

Figure 2 shows the change of LFS with the pressure and temperature of unburned stoichiometric H_2/air. It is observed that the results from three chamber sizes of $R_W = 1$, 5 and 10 cm overlap. According to Figure 1 and Equation (5), the relative PRR for $R_W = 1\,\text{cm}$ is ten times of that for $R_W = 10\,\text{cm}$. Therefore, Figure 2 indicates that the PRR has little effect on LFS. This conclusion is further demonstrated by Figure 3, which plots the LFS as a function of relative PRR. The relative deviation of each LFS (symbols in Figure 3) from the averaged value (the lines) is within 0.3%.

Figure 4 compares the flame structures at four values of K_P but the same pressure and unburned gas temperature, $P = 4\,\text{atm}$ and $T_u = 444\,\text{K}$. Zero K_P is obtained from simulating flame propagation in a spherical chamber with $R_W = 50\,\text{cm}$ and for stoichiometric H_2/air initially at $P_0 = 4\,\text{atm}$ and $T_{u,0} = 444\,\text{K}$. The flame radius is at $R_f = 4.62\,\text{cm}$ and

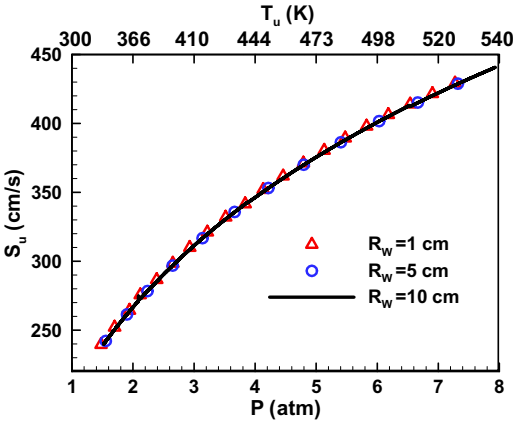

Figure 2. Change of LFS with the pressure and temperature of unburned stoichiometric H_2/air initially at $T_{u,0} = 300$ K and $P_0 = 1$ atm.

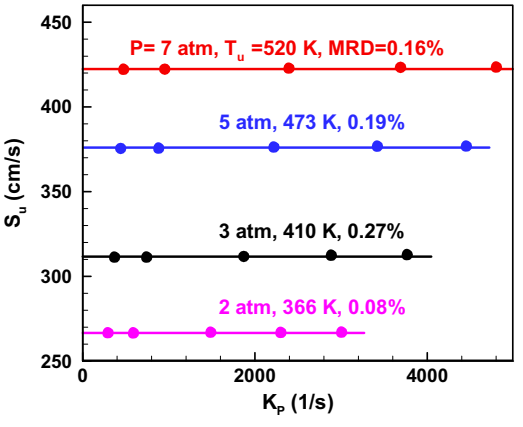

Figure 3. Change of local LFS, S_u, with the relative PRR for stoichiometric H_2/air at different pressures and temperatures. For each set of pressure and temperature, the symbols from left to right correspond to chamber size of $R_W = 10$, 5, 2, 1.3 and 1 cm, respectively. The horizontal lines represent the averaged values of S_us at the same set of (P, T_u). The maximum relative difference (MRD) from the averaged value of five points is shown above the lines.

the pressure rise is negligible. The other three values of K_p correspond to three chamber radii of $R_W = 1$, 2 and 10 cm and the mixture is initially at $P_0 = 1$ atm and $T_{u,0} = 300$ K. The condition of $P = 4$ atm and $T_u = 444$ K is reached after the unburned gas is compressed by flame propagation inside the closed chamber. Figure 4(a,b) show that the states of burnt gas are affected by the relative PRR. The higher the K_P, the larger the gradients of temperature and OH mass fraction in the burnt gas region. However, Figure 4(a,b) show that at the flame front, the local temperature and OH mass fraction are not affected by the relative PRR. Moreover, Figure 4(c) shows that the heat release rate also remains nearly the same for these four values of K_P. Therefore, the PRR has little effect on the reaction zone. This explains why the PRR has little effect on flame speed.

The above results are for stoichiometric H_2/air initially at $T_{u,0} = 300$ K and $P_0 = 1$ atm. The corresponding maximum unburned gas temperature and pressure (around 550 K

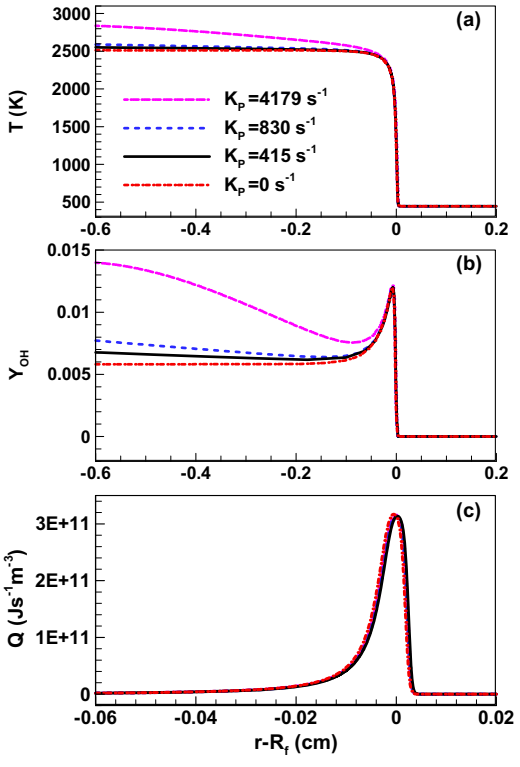

Figure 4. Distributions of temperature (a), mass fraction of OH (b) and heat release rate (c) for premixed H_2/air flames at different values of relative PRR but the same pressure and temperature for the unburned mixture ($P = 4$ atm, $T_u = 444$ K). Note that the horizontal axis in (c) is enlarged by ten times since the reaction zone is very thin.

and 8 atm) are below those under engine-relevant conditions. The influence of PRR on LFS at engine-relevant condition is also examined. The results for H_2/air, CH_4/air and iC_8H_{18}/air under engine-relevant conditions are shown in Figures S4–S6 in the Supplementary Document, which demonstrates that the effect of PRR on LFS is also negligible under these engine-relevant conditions.

Since iC_8H_{18}/air has much lower LFS than that of H_2/air, its PRR is also much smaller than that of H_2/air. To achieve high PRR, in simulation we artificially multiply both the reaction rates and thermal and mass diffusivities by ten so that the LFS is enlarged by around ten times. This also mimics the turbulence which accelerates flame propagation in ICEs. The results for artificially accelerated iC_8H_{18}/air flame are shown in Figure 5. For $R_W = 1$ cm, K_P reaches 7000 s^{-1} which is close to the value in SIEs. As shown in Figure 6, the relative deviation from the averaged value is within 0.4%. Therefore, the PRR has little effect on LFS under engine-relevant condition.

5. Analysis on the unsteady effects based on the temperature equation

To explain the above simulation results which show that the PRR has little effect on LFS, we analyse the unsteady effects based on the following energy/temperature equation for an

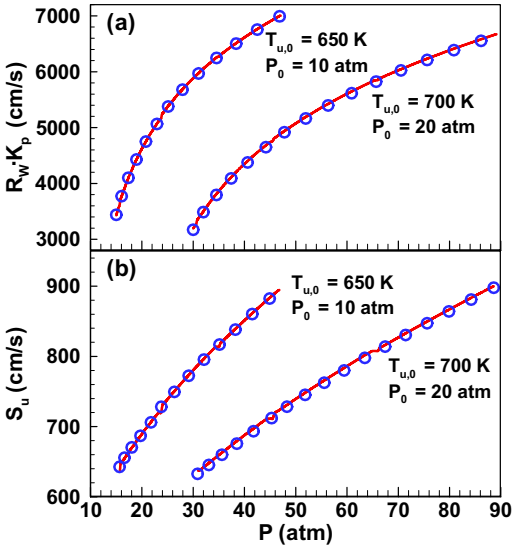

Figure 5. Change of R_W K_P (a) and S_u (b) with P of unburned stoichiometric iC_8H_{18}/air mixture initially at ($T_{u,0} = 650$ K, $P_0 = 10$ atm) and ($T_{u,0} = 700$ K, $P_0 = 20$ atm). The unburned gas temperature is determined from pressure according to the isentropic-compression relationship. The lines and symbols represent results for $R_W = 1$ and 5 cm, respectively. The flame is artificially accelerated through multiplying both the reaction rates and thermal and mass diffusivities by 10.

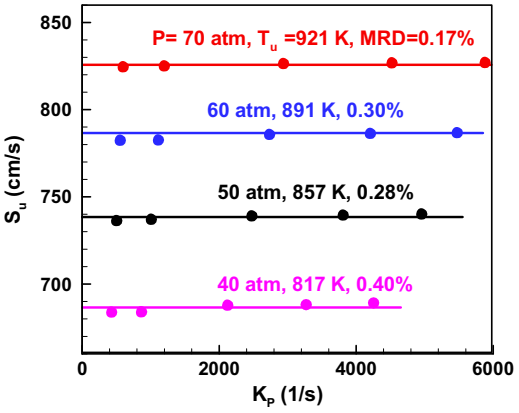

Figure 6. Change of local LFS, S_u, with the relative PRR, K_P, for stoichiometric iC_8H_{18}/air at different pressures and temperatures. For each set of pressure, P, and temperature, T_u, the symbols from left to right correspond to chamber size of $R_W = 10$, 5, 2, 1.3 and 1 cm, respectively. The horizontal lines represent the averaged values of $S_u s$ at the same set of (P, T_u). The maximum relative difference (MRD) from the averaged value of five points is shown above the lines.

adiabatic, planar, premixed flame:

$$\rho C_P \left(\frac{\partial T}{\partial t} + u \frac{\partial T}{\partial x} \right) = \frac{\partial}{\partial x} \left(\lambda \frac{\partial T}{\partial x} \right) + \frac{\mathrm{d}P}{\mathrm{d}t} + \omega_T \tag{6}$$

where ω_T is the chemical heat release rate, C_P the heat capacity, and λ the thermal conductivity of the mixture.

In the preheat zone of a premixed flame, the convective term balances with the diffusion term. To assess the unsteady effects due to pressure rise, we only need compare the pressure rise term, dP/dt, with the convection term in Equation (6). Their ratio can be assessed as

$$\left(\frac{\mathrm{d}P}{\mathrm{d}t}\right)\Big/\left(\rho C_P u\frac{\partial T}{\partial x}\right)\sim\left(\frac{R}{C_P}\right)\left(\frac{\mathrm{d}P}{P\mathrm{d}t}\right)\Big/\left(\frac{S_u}{T_u}\frac{T_{ad}-T_u}{l_f}\right) \tag{7}$$

in which T_{ad} is the adiabatic flame temperature and l_f is the flame thickness evaluated based on maximum temperature gradient [27]. The equation of state, $P=\rho RT$, is used. Substituting the relationship of $C_P=\gamma_u R/(\gamma_u-1)$ into Equation (7) yields:

$$\left(\frac{\mathrm{d}P}{\mathrm{d}t}\right)\Big/\left(\rho C_P u\frac{\partial T}{\partial x}\right)\sim\frac{(1-1/\gamma_u)}{(T_{ad}/T_u-1)}\frac{K_P}{(S_u/l_f)} \tag{8}$$

Jayachandran and Egolfopoulos [27] interpreted the unsteady effect of pressure rise through comparing the time scale of unsteady pressure rise and that of the premixed flame. The characteristic time for unsteady pressure rise is $t_P=1/K_P$ and that for premixed flame is $t_f=l_f/S_u$ [27]. We introduce the Damköhler number, which is defined as $Da=t_P/t_f=S_u/(K_P l_f)$. Therefore, Equation (8) becomes

$$\left(\frac{\mathrm{d}P}{\mathrm{d}t}\right)\Big/\left(\rho C_P u\frac{\partial T}{\partial x}\right)\sim\frac{g}{Da}\quad\text{with}\quad g=\frac{1-1/\gamma_u}{T_{ad}/T_u-1} \tag{9}$$

The factor, g, is 0.04 and 0.087 for stoichiometric iC_8H_{18}/air mixture initially at ($T_{u,0}=300\,\mathrm{K}$, $P_0=1\,\mathrm{atm}$) and ($T_{u,0}=700\,\mathrm{K}$, $P_0=20\,\mathrm{atm}$), respectively. The Damköhler number is plotted in Figure 7 for $R_W=1\,\mathrm{cm}$. Compared to $R_W=1\,\mathrm{cm}$, Da for $R_W=5\,\mathrm{cm}$ is about five times larger since K_P for $R_W=5\,\mathrm{cm}$ is five times smaller as shown by Equation (5) and Figure 1. Since $g<0.1$ and $Da>50$, Equation (9) shows that the ratio between the unsteady and convective terms in the temperature equation is very small. Therefore, the unsteady pressure rise term in Equation (6) can still be neglected for the PRR considered in this work. This indicates that the flame structure does not have enough time to respond to the pressure variation, and thereby explains that the PRR has little effect on LFS.

The Damköhler number defined here is the same as the inverse of pressure rise number, $\mathrm{PRN_f}$, proposed by Jayachandran and Egolfopoulos [27], i.e., $Da=1/\mathrm{PRN_f}$. It is also similar to the dimensionless time scale parameter used in the analysis of flame response to pressure disturbances [41,42]. In [27], the largest pressure rise number is around 2 and thereby their smallest Damköhler number is about 0.5, which is much lower than the value shown in Figure 7. For a Damköhler number in the order of unity, Da 1, the ratio g/Da is in the same order of the inverse of Zel'dovich number (usually in the range of 7–12) and Equation (9) indicates that the unsteady effects might not be negligible. Consequently, the transient pressure rise can affect the LFS as shown by Jayachandran and Egolfopoulos [27]. In fact, the maximum relative PRR in this work is much lower than that in [27]. Besides, the present results are consistent with those in [41,42] which shows that the premixed flame is only sensitive to pressure disturbances with very high frequency. Nevertheless, only scaling analysis is presented above, and currently we cannot derive an analytical expression to quantify the pressure rise effect on the laminar flame speed through a more formal analysis.

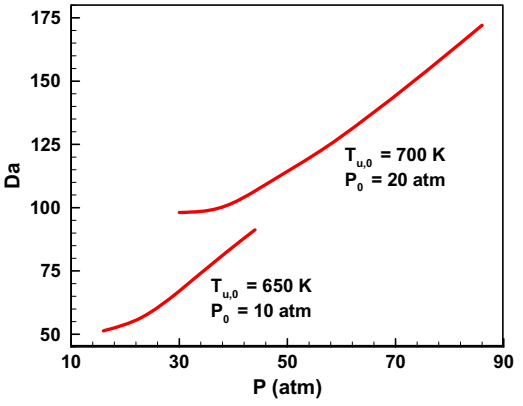

Figure 7. Change of Da with P of unburned stoichiometric iC_8H_{18}/air mixture initially at ($T_{u,0} = 650\,\text{K}$, $P_0 = 10\,\text{atm}$) and ($T_{u,0} = 700\,\text{K}$, $P_0 = 20\,\text{atm}$). The unburned gas temperature is determined from pressure according to the isentropic-compression relationship. The chamber radius is $R_W = 1\,\text{cm}$. The flame is artificially accelerated through multiplying both the reaction rates and thermal and mass diffusivities by 10.

6. Other comments

In experiments on constant-volume propagating spherical flames, it is very difficult to achieve the high PRR comparable to that obtained in our simulation. Metghalchi and coworkers [18,20,43] performed experiments for the same mixture but different initial pressures and temperatures along specific isentropic lines. A thermodynamic state (same pressure and unburned gas temperature) that is shared by all different experiments was selected to demonstrate that the stretch effects are negligible. In fact, at such thermodynamic state, not only the stretch but also the pressure rise rate changes for different initial pressures and temperatures along specific isentropic lines. Therefore, the experiments conducted by Metghalchi and coworkers [18,20,43] also indicate that the effects of stretch and unsteady pressure rise on the LFS are negligible for conditions considered in their studies.

Usually the stretch rate, K_S or K_C, in the order of $1000\,\text{s}^{-1}$ can have great impact on flame speed. To get accurate LFS, linear or nonlinear extrapolation to zero stretch rate needs to be conducted [2–4]. However, as shown by Figures 3 and 6, the relative PRR, K_P, in the order of $1000\,\text{s}^{-1}$, has little effect on flame speeds. This is because the stretch and PRR affects the premixed flame differently. The PRR brings the unsteady effects as discussed in Section 5. However, the stretch can affect the energy balance inside the flame structure for steady or quasi-steady premixed flames [7,10,12]. At very high PPR, the energy balance inside the flame could be affected by unsteady pressure rise. The present results show that the magnitude of L_P in Equation (1) is not in the same order as those of L_s and L_c. In fact Figures 3 and 6 indicate that the value of L_P in Equation (1) is almost zero.

It is noted that the stretch effect can be completely prevented by considering a propagating planar flame rather than a propagating spherical flame. However, we need use a small chamber size of 1 cm to achieve high PRR, for which the ignition effect in a planar geometry is strong. In order to diminish the ignition effect [30,44] we consider the spherical geometry rather than the planar geometry. The stretch effect might couple with the effect of unsteady pressure rise. Here the combined effects of stretch and PRR is expected to be negligible.

7. Conclusions

One-dimensional transient simulations are conducted for different fuels to assess the effects of PRR on LFS at normal and engine-relevant conditions. The relative PRR is shown to be inversely proportional to the chamber size. High relative PRR is achieved by reducing the chamber size. Simulation results show that the PRR has little effect on the reaction zone and LFS. This is explained through the analysis of the energy equation for a premixed flame which shows that the unsteady term is negligible for the PRR considered in this work. This study demonstrates that the effect of unsteady pressure rise on the LFS measured from the constant-volume propagating spherical flame method is negligible. Furthermore, the high PRR has little influence on premixed flame propagation in SIEs.

It is noted that the above conclusions hold only for cases that there is no autoignition in the unburned gas. It has been found that autoignition in the unburned gas can greatly change the flame propagation speed [45–47]. Further study needs to be conducted to understand how the premixed flame propagation is affected by the coupling between unsteady pressure rise rate and autoignition in the unburned gas, which might occur in boosted gasoline engines.

Acknowledgements

This work was supported by National Natural Science Foundation of China (Nos. 91741126 and 51861135309). Z.C. thanks Mr. Ziyu Wang at Northeastern University for helpful discussion on laminar flame speeds measured from constant-volume propagating spherical flames. Z.C. also thanks Prof. Paul Clavin at Aix-Marseille Université for helpful discussion on the results shown in Section 6.

Disclosure statement

No potential conflict of interest was reported by the author(s).

Funding

This work was supported by National Natural Science Foundation of China [grant numbers 91741126 and 51861135309].

Supplemental data

Supplemental data for this article can be accessed at https://doi.org/10.1080/13647830.2020.1780325.

ORCID

Zheng Chen http://orcid.org/0000-0001-7341-6099

References

[1] G.E. Andrews and D. Bradley, *Determination of burning velocities: A critical review*, Combust. Flame. 18 (1972), pp. 133–153.
[2] F.N. Egolfopoulos, N. Hansen, Y. Ju, K. Kohse-Hoinghaus, C.K. Law, and F. Qi, *Advances and challenges in laminar flame experiments and implications for combustion chemistry*. Prog. Energy Combust. Sci. 43 (2014), pp. 36–67.

[3] Z. Chen, *On the accuracy of laminar flame speeds measured from outwardly propagating spherical flames: Methane/air at normal temperature and pressure*. Combust. Flame 162 (2015), pp. 2442–2453.

[4] A.A. Konnov, A. Mohammad, V.R. Kishore, N.I. Kim, C. Prathap, and S. Kumar, *A comprehensive review of measurements and data analysis of laminar burning velocities for various fuel plus air mixtures*. Prog. Energy Combust. Sci. 68 (2018), pp. 197–267.

[5] C.K. Wu and C.K. Law, *On the determination of laminar flame speed from stretched flames*. Proc. Combust. Inst. 20 (1985), pp. 1941–1949.

[6] D. Bradley, P.H. Gaskell and X.J. Gu, *Burning velocities, Markstein lengths, and flame quenching for spherical methane-air flames: A computational study*. Combust. Flame 104 (1996), pp. 176–198.

[7] C.K. Law and C.J. Sung, *Structure, aerodynamics, and geometry of premixed flamelets*. Prog. Energy Combust. Sci. 26 (2000), pp. 459–505.

[8] F. Halter, T. Tahtouh and C. Mounaïm-Rousselle, *Nonlinear effects of stretch on the flame front propagation*. Combust. Flame 157 (2010), pp. 1825–1832.

[9] Z. Chen, *On the extraction of laminar flame speed and Markstein length from outwardly propagating spherical flames*. Combust. Flame 158 (2011), pp. 291–300.

[10] P. Clavin, *Dynamic behavior of premixed flame fronts in laminar and turbulent flows*. Prog. Energy Combust. Sci. 11 (1985), pp. 1–59.

[11] P. Clavin and J.C. Grana-Otero, *Curved and stretched flames: The two Markstein numbers*. J. Fluid. Mech. 686 (2011), pp. 187–217.

[12] P. Clavin and G. Searby, *Combustion Waves and Fronts in Flows*, Cambridge University Press, Cambridge, 2016.

[13] P. Clavin and G. Joulin, *Turbulent Reactive Flows*, Springer, New York, 1989213240.

[14] S.M. Candel and T.J. Poinsot, *Flame stretch and the balance equation for the flame area*. Combust. Sci. Tech. 70 (1990), pp. 1–15.

[15] M. Metghalchi and J.C. Keck, *Laminar burning velocity of propane-air mixtures at high-temperature and pressure*. Combust. Flame 38 (1980), pp. 143–154.

[16] K. Saeed and C.R. Stone, *Measurements of the laminar burning velocity for mixtures of methanol and air from a constant-volume vessel using a multizone model*. Combust. Flame 139 (2004), pp. 152–166.

[17] S.P. Marshall, S. Taylor, C.R. Stone, T.J. Davies and R.F. Cracknell, *Laminar burning velocity measurements of liquid fuels at elevated pressures and temperatures with combustion residuals*. Combust. Flame 158 (2011), pp. 1920–1932.

[18] K. Eisazadeh-Far, A. Moghaddas, J. Al-Mulki and H. Metghalchi, *Laminar burning speeds of ethanol/air/diluent mixtures*. Proc. Combust. Inst. 33 (2011), pp. 1021–1027.

[19] M. Kuznetsov, R. Redlinger, W. Breitung, J. Grune, A. Friedrich and N. Ichikawa, *Laminar burning velocities of hydrogen-oxygen-steam mixtures at elevated temperatures and pressures*. Proc. Combust. Inst. 33 (2011), pp. 895–903.

[20] O. Askari, A. Moghaddas, A. Alholm, K. Vien, B. Alhazmi and H. Metghalchi, *Laminar burning speed measurement and flame instability study of H_2/CO/air mixtures at high temperatures and pressures using a novel multi-shell model*. Combust. Flame 168 (2016), pp. 20–31.

[21] C. Xiouris, T. Ye, J. Jayachandran and F.N. Egolfopoulos, *Laminar flame speeds under engine-relevant conditions: Uncertainty quantification and minimization in spherically expanding flame experiments*. Combust. Flame 163 (2016), pp. 270–283.

[22] N. Hinton, R. Stone and R. Cracknell, *Laminar burning velocity measurements in constant volume vessels – reconciliation of flame front imaging and pressure rise methods*. Fuel 211 (2018), pp. 446–457.

[23] R.R. Burrell, J.L. Pagliaro and G.T. Linteris, *Effects of stretch and thermal radiation on difluoromethane/air burning velocity measurements in constant volume spherically expanding flames*. Proc. Combust. Inst. 37 (2019), pp. 4231–4238.

[24] M. Faghih and Z. Chen, *The constant-volume propagating spherical flame method for laminar flame speed measurement*. Sci. Bull 61 (2016), pp. 1–15.

[25] G. Xu, C. Hanauer, Y. Wright and K. Boulouchos, *CFD-simulation of ignition and combustion in lean burn gas engines*, SAE Paper (2016) 2016-01-0800.

[26] Z.C. Tan and R.D. Reitz, *An ignition and combustion model based on the level-set method for spark ignition engine multidimensional modeling*. Combust. Flame 145 (2006), pp. 1–15.

[27] J. Jayachandran and F.N. Egolfopoulos, *Effect of unsteady pressure rise on flame propagation and near-cold-wall ignition*. Proc. Combust. Inst. 37 (2019), pp. 1639–1647.
[28] I. Smith, C.K. Westbrook and R.F. Sawyer, *Lean limit combustion in an expanding chamber*. Seventeenth Symp. (Int.) Combust. 17 (1979), pp. 1305–1313.
[29] N. Peters and G.S.S. Ludford, *The effect of pressure variations on premixed flames*. Combust. Sci. Tech. 34 (1983), pp. 331–344.
[30] Z. Chen, M.P. Burke, and Y. Ju, *Effects of Lewis number and ignition energy on the determination of laminar flame speed using propagating spherical flames*. Proc. Combust. Inst 32 (2009), pp. 1253–1260.
[31] Z. Chen, *Effects of radiation and compression on propagating spherical flames of methane/air mixtures near the lean flammability limit*. Combust. Flame 157 (2010), pp. 2267–2276.
[32] P. Dai and Z. Chen, *Supersonic reaction front propagation initiated by a hot spot in n-heptane/air mixture with multistage ignition*. Combust. Flame 162 (2015), pp. 4183–4193.
[33] J. Li, Z. Zhao, A. Kazakov, and F.L. Dryer, *An updated comprehensive kinetic model of hydrogen combustion*. Int. J. Chem. Kinet. 36 (2004), pp. 566–575.
[34] G. Smith, D. Golden, and M. Frenklach, The GRI-Mech 3.0 chemical kinetic mechanism. Available at https://combustion.berkeley.edu/gri-mech/.
[35] M. Chaos, A. Kazakov, Z. Zhao, and F.L. Dryer, *A high-temperature chemical kinetic model for primary reference fuels*. Int. J. Chem. Kinet. 39 (2007), pp. 399–414.
[36] W.K. Zhang, X.L. Gou, and Z. Chen, *Effects of water vapor dilution on the minimum ignition energy of methane, n-butane and n-decane at normal and reduced pressures*. Fuel 187 (2017), pp. 111–116.
[37] M. Faghih and Z. Chen, *Two-stage heat release in nitromethane/air flame and its impact on laminar flame speed measurement*. Combust. Flame 183 (2017), pp. 157–165.
[38] W.K. Zhang, M. Faqih, X.L. Gou, and Z. Chen, *Numerical study on the transient evolution of a premixed cool flame*. Combust. Flame 187 (2018), pp. 129–136.
[39] Z. Li, X. Gou and Z. Chen, *Effects of hydrogen addition on non-premixed ignition of iso-octane by hot air in a diffusion layer*. Combust. Flame 199 (2019), pp. 292–300.
[40] Y. Wang, A. Movaghar, Z. Wang, Z. Liu, W. Sun, F.N. Egolfopoulos, and Z. Chen, *Laminar flame speeds of methane/air mixtures at engine conditions: Performance of different kinetic models and power-law correlations*. Combust. Flame 218 (2020), pp. 101–108.
[41] A.C. Mcintosh, *Pressure disturbances of different length scales interacting with conventional flames*, Combust. Sci. Tech. 75 (1991), pp. 287–309.
[42] T.C. Lieuwen, *Unsteady Combustion Physics*, Cambridge University Press, New York, 2012.
[43] Z.Y. Wang, Z.W. Bai, S.C. Yelishala, G.Y. Yu, and H. Metghalchi, *Effects of diluent on laminar burning speed and flame structure of gas to liquid fuel air mixtures at high temperatures and moderate pressures*. Fuel 231 (2018), pp. 204–214.
[44] Z. Chen, M.P. Burke, and Y. Ju, *On the critical flame radius and minimum ignition energy for spherical flame initiation*. Proc. Combust. Inst 33 (2011), pp. 1219–1226.
[45] H. Yu and Z. Chen, *End-gas autoignition and detonation development in a closed chamber*. Combust. Flame 162 (2015), pp. 4102–4111.
[46] M. Faghih, H.Y. Li, X.L. Gou, and Z. Chen, *On laminar premixed flame propagating into autoigniting mixtures under engine-relevant conditions*. Proc. Combust. Inst 37 (2019), pp. 4673–4680.
[47] A. Ansari, J. Jayachandran, and F.N. Egolfopoulos, *Parameters influencing the burning rate of laminar flames propagating into a reacting mixture*. Proc. Combust. Inst 37 (2019), pp. 1513–1520.